CAMBRIDGE
UNIVERSITY PRESS

RESEARCH ARTICLE

Theoretical study on a modified rocker-bogie suspension for robotic rovers

Chiara Cosenza, Vincenzo Niola, Stefano Pagano and Sergio Savino [iD]

Department of Industrial Engineering, University of Naples – Federico II, Napoli, Italy
Corresponding author: Sergio Savino; Email: sergio.savino@unina.it

Abstract

Robotic rovers equipped with articulated rocker-bogie suspension have aroused great interest after the explorations on Mars; this interest has also shifted to different types of terrestrial applications such as in the agriculture, military, and rescue fields. The suspension can be designed so that, when the rover is on flat and horizontal ground, the weight is evenly distributed among the wheels; in this way, all wheels have the same traction capability and offer the same rolling resistance. As the operating conditions vary due to sloping ground, uneven ground surface, or different payload position, the weight distribution can undergo considerable variations. This type of suspension is statically determined with respect to weight, but it is indeterminate with respect to traction forces; the traction control system aims to avoid the wheels slippage. In this paper, the traction contribution that each wheel can provide, to overcome a step obstacle, is shown. Furthermore, the possibility of regulating the distribution of vertical loads among the wheels adopting a torsion spring, with adjustable preload, arranged between rocker and bogie, is evaluated. A suitable spring preload facilitates the initial phase of the obstacle overcoming if the rover advances with the bogie forward. Numerical simulations show that to increase the possibility of overcoming an obstacle it is sufficient for the spring preload to reduce the vertical load on the front wheel; in any case, a higher load variation would not be advisable as it could involves an excessive load difference among the wheels.

1. Introduction

Planetary rovers are mobile robots designed to move slowly on the rough surface of a body in the solar system, other than the Earth, to collect information on the characteristics of the environment. The first mobile robot adopted for planetary explorations on the Moon was Lunokhod; it was developed by the Soviets in 1970 [1] and was characterized by eight driving wheels connected to the chassis by means of an articulated suspension system. One year later, the Americans sent on the Moon the Apollo 15 rover having four wheels and an elastic suspension system. Generally, in the field of robot rover, "articulated suspensions" refer to passive kinematic suspension systems based on linkages that allow the wheels to move with respect to the chassis following the geometry of the ground; they differ from dynamic (or elastic) suspension systems which also include springs and dampers and are mainly adopted when a quick response is needed to ensure that the wheel is able to follow the profile of the ground without detaching from it. One of the problems that the rover developers had to solve was the contact between the wheels of rovers and the unevenness soil of the Moon whose characteristics were unknown. Similarly to what happens for off-road vehicles, there was the risk of encountering solid obstacles to overcome or areas with incoherent soil with the risk of sinking the wheels. The suspension system had to guarantee a fair equal distribution of the vertical load among the wheels, so that each of them could have good traction capacity and the same flotation capacity on soft soils.

Elastic suspensions turned out to be less suitable for this application as they can generate high load disparities among the wheels if one of them engages with an obstacle. In fact, if only one wheel is in a
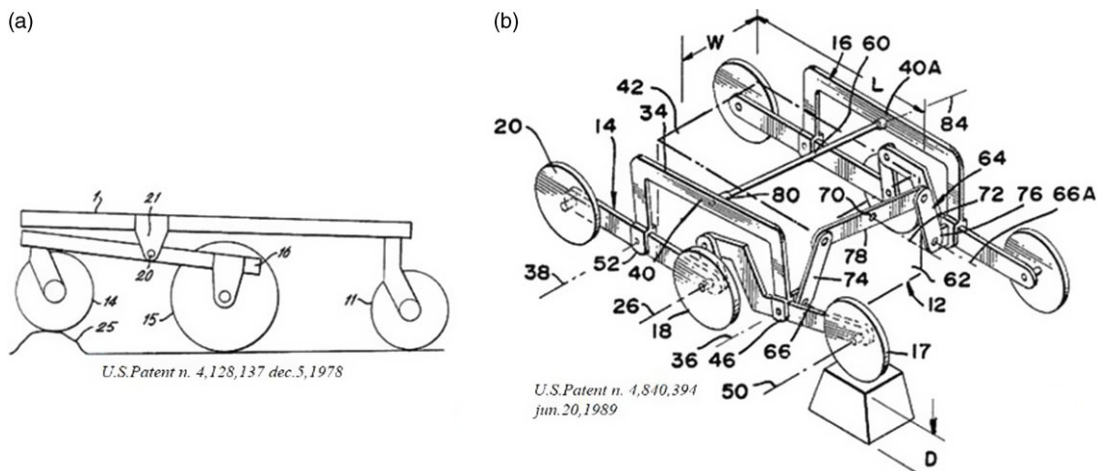
Figure 1. *Articulated suspension: (a) Peripatetic vehicle (U.S. Patent n. 4,128,137 dec.5,1978); (b) NASA articulated suspension (U.S. Patent n. 4,840,394 jun.20,1989).*

more depressed area, the corresponding elastic suspension will extend to allow the wheel to lie below the level of the other wheels; in this condition, the wheel lying in the depressed area will provide a minor contribution to support the vehicle weight which will be, therefore, shared among the other wheels. This condition has the negative consequence of having an unloaded wheel with no traction capacity and the other wheels (more loaded) with a greater tendency to sink. It is possible to reduce this effect, within certain limits, by using low stiffness suspensions with a longer stroke, but this would lead to undesirable low frequency natural oscillations and large static deformations. Furthermore, the elastic systems determine a high variation in height compared to the articulated ones.

The rovers used by NASA, since 1997, for Mars explorations have six wheels and are all equipped with articulated suspension; currently, this configuration is considered to be the optimal one for the ability to overcome obstacles. Thanks to the ability to adapt to uneven ground, it allows the load to be distributed fairly evenly among the wheels so that each of them can contribute to supporting the load and can have a good traction capacity avoiding that one of them has an evident greater tendency to sink. This type of suspension is also appreciable for its reduced weight and size.

Similar suspension system had already been adopted for the "peripatetic vehicles" (1978) [2] equipped with a two-wheeled bogie, connected to the vehicle chassis (Fig. 1(a)) and a rear castored wheel to give the vehicle higher maneuverability [3]. The two central wheels are driven by independent motors to allow the vehicle to steer in a differential way.

In 1989, Donald B. Bickler (NASA Pasadena Office CA) patented [4] an articulated suspension system (Fig. 1(b)) for space explorations rovers [5]. It was designed with the aim to equally distribute the vertical load among the wheels and to reduce the body pitch angle. The articulated system scheme proposed by Bickler was modified several times, and the final configuration, known as *rocker-bogie* suspension [6, 7], was adopted for the Sojourner rover [8, 9] in the Pathfinder mission to Mars (1997).

This type of rover, schematically represented in Fig. 2, has six driving wheels connected to the body of the rover by means of a statically determined mechanical linkage; on each side of the rover, there is a rocker supporting a wheel, joined to a two-wheeled bogie by means of a passive rotational joint. A differential mechanism connects the two rockers, imposing them opposite rotations so allowing the body to perform reduced pitch rotations, equal to the average pitch angle of two rockers, thus reducing even the rover overturning risk.

The dimensions of the wheels and the lengths of the suspension links are chosen according to the dimensions of the obstacles to be overcome [10] and the mission characteristics [11]; the length of the links can also be chosen so that the vertical load is equally distributed among the wheels when the
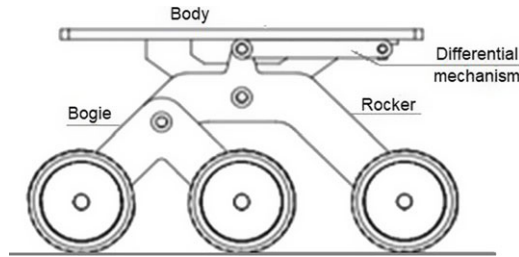
Figure 2. *Rover with rocker-bogie suspension.*

rover is on a flat horizontal surface; in this way, the pressure on the ground, the sinking, and the driving capacity are quite the same for all the wheels. However, due to the ground unevenness or to a different payload position, the load distribution may be altered. In these conditions, ground reactions on the rover wheels may be defined by means of a preliminary position kinematic analysis to derive the configuration of the rover members according to the geometry of the ground profile [12, 13]. Thanks to the very low speed (about 2 cm/s), the ground reactions can be determined by means of static analysis as accelerations assume negligible values. In the static analysis, the suspension links are considered rigid.

It was evaluated that vehicles with six wheels, although more complex and heavier than a four-wheeled vehicle, have a greater ability to overcome obstacles [14]. A higher number of wheels would make the obstacle overcoming easier, but the vehicle weighs increment associated with mechanical, control, and steering complexity make the solution less practical. In ref. [15], some metrics are established, that is, a set of indicators to be used to evaluate and compare different types of suspension and identify the one that best meets the requirements of a mission. With reference to the characteristics of space missions, the study highlights that a four-wheeled rover can be a valid alternative to a six-wheeled rover only in very specific missions.

At the present, the rocker-bogie system still appears to be the simplest and the most reliable suspension system. It has even a good ability to overcome large holes and obstacles whose heights can be approximately equal to the radius of the wheel, although they can also overcome obstacles of higher size. Furthermore, it can be folded allowing for a much smaller stowage volume than the operational one [16].

For this reason, this kind of suspension is adopted even in terrestrial applications as in the agricultural and military fields, in civil protection operations, etc. [17].

Considering the wheel load variation due to the soil irregularities or the payload position variation, in this paper, it has evaluated the possibility of introducing a torsion spring, with adjustable preload, between the rocker and the bogie, to change the load distribution among the wheels according to the mission characteristics and the payload center of gravity position [18]. In this way, it is possible to reduce the load on the front wheels so that they can overcome obstacles more easily. To this end, reactions exerted by the ground on the wheels are analytically determined in function of the spring preload value. The analytical results are a guide for the numerical simulations conducted by means of multiphysics modeling [19].

2. Load distribution among wheels on a flat and horizontal ground

Rovers adopted for spatial missions are meant to move at very low forward speeds; in this condition, the acceleration due to the ground unevenness may be neglected. The rocker-bogie suspension is designed so that the rover weight is equally distributed among the wheels when it moves on a flat and horizontal ground; to this end, the dimensions of the suspension can be chosen as indicated in the planar scheme of Fig. 3, which represents the articulated suspension without the chassis. In the scheme, it is assumed that the whole mass is lumped in point D of the rocker, placed on the vertical direction of the center of
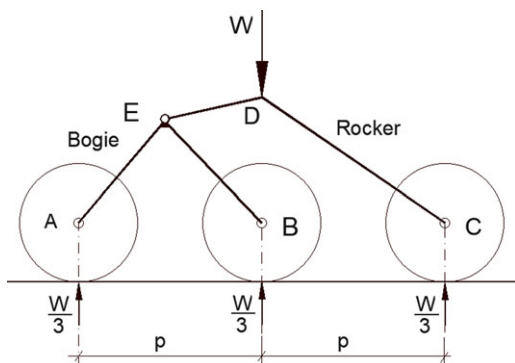
Figure 3. *Nominal static load distribution.*
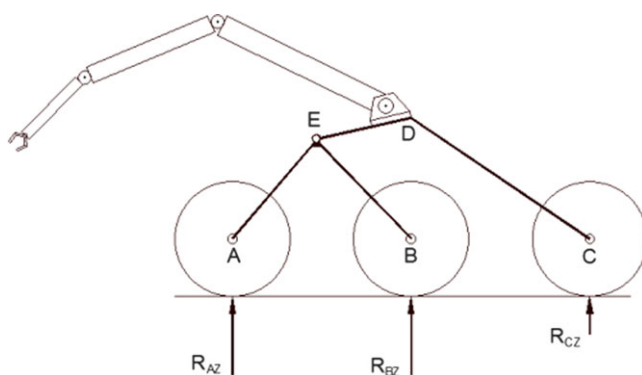
Figure 4. *Rover equipped with a robotic arm.*

wheel B and that the distance p, between two consecutive wheels, is the same when the wheels are at the same level. In this configuration, it can be assumed that each wheel can exert the same traction force.

The position of the center of mass may not coincide with point D or it may vary with the position of the payload as it happens, for example, if rover is equipped with a robotic arm (Fig. 4); in this case, the load distribution among the wheels is no longer the same even if the wheels are on a flat and horizontal plane.

The articulated suspension is connected to the chassis (or body) by hinge D and by the horizontal rod that connects point G of the suspension to point H of the body (Fig. 5).

The moment of the weight ($W \cdot e$) is balanced by the horizontal reaction forces N acting in hinges H and D. In case of flat and horizontal ground, the vertical ground reactions are:

$$R_{AZ} = R_{BZ} = \frac{W}{3}\left(1 + \frac{e}{p}\right); R_{CZ} = \frac{W}{3}\left(1 - 2\frac{e}{p}\right) \tag{1}$$

In the following, it is assumed that the eccentricity of the weight, *e,* is null so that the three ground reactions are equal in case of flat and horizontal ground. The load distribution among the wheels may vary if they are not at the same level or if the ground surface is irregular or if one of the wheels approaches an obstacle. In these cases, the less-loaded wheels provide a reduced traction force as they tend to slip.
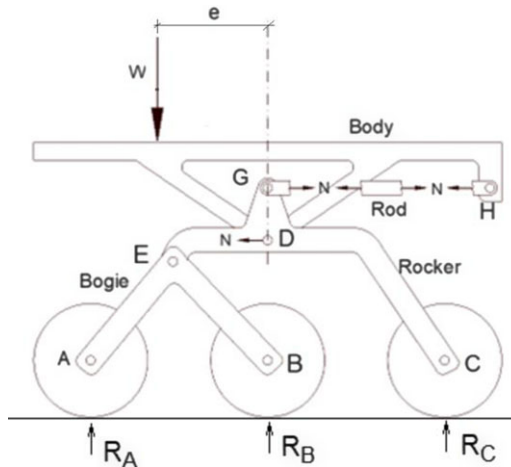
Figure 5. *Eccentric payload on the body.*

2.1 Load distribution among wheels on uneven soil

If the wheels are on uneven soil, the ground vertical reactions may be evaluated by performing a preliminary kinematic position analysis considering the bidimensional model of the suspension (Fig. 6). The analysis is based on the knowledge of:

- suspension geometry characterized by the lengths of the links, L_i, the wheel radius, r, the rocker angles, β, and the bogie angle, γ;
- the ground profile defined by the heights of the contact points, h_i, the angle between the wheel-ground common tangent line, and the reference x axis, α_i.

The linkage configuration is described by the angles θ_i that the suspension links form with the reference axis x, considering that:

$$\theta_2 = \theta_1 + \gamma; \theta_3 = \theta_4 + \beta; \psi = \theta_1 - \theta_4 \tag{2}$$

where ψ is the angle between rocker and bogie.
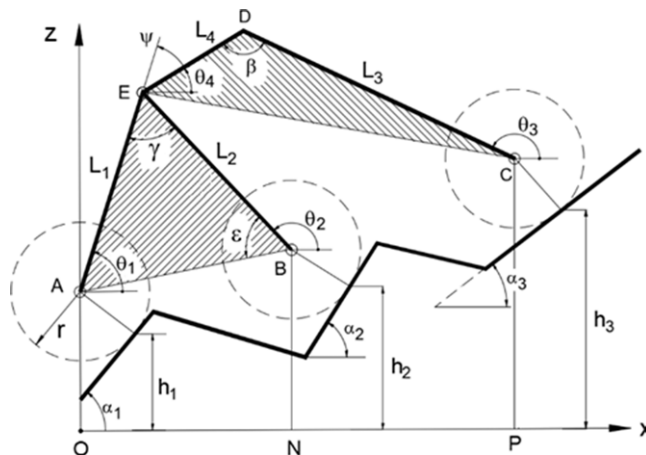
Figure 6. *Suspension kinematic scheme. The wheel-ground contact points are characterized by height hi; the common tangent is inclined by an angle α_i.*

The ordinates of points A, B, C, D, E are:

$$z_A = h_1 + r \cos \alpha_1; \ z_B = h_2 + r \cos \alpha_2; \ z_C = h_3 + r \cos \alpha_3$$

$$z_D = z_C + L_3 \sin \theta_3; \ z_E = z_A + L_1 \sin \theta_1 \tag{3}$$

Considering the projection along the vertical direction of the vectors arranged along the sides of the polygons OAEBN and NBEDCP, the following two scalar equations are obtained:

$$(h_1 + r \cos \alpha_1) + L_1 \sin \theta_1 = (h_2 + r \cos \alpha_2) + L_2 \sin \theta_2 \tag{4}$$

$$(h_2 + r \cos \alpha_2) + L_2 \sin \theta_2 + L_4 \sin \theta_4 = (h_3 + r \cos \alpha_3) + L_3 \sin \theta_3 \tag{5}$$

Both equations can be expressed in the synthetic form as: $A \sin \theta_i + B \cos \theta_i + C = 0$
Being:
Eq. (4):

$$\theta_i = \theta_2; A = L_1 - L_2 \cos\gamma; B = -L_2 \sin\gamma; C = (h_1 - h_2) + r(\cos \alpha_1 - \cos \alpha_2) \tag{6}$$

Eq. (5):

$$\theta_i = \theta_3; A = L_3 - L_4 \cos\beta; B = L_4 \sin \beta; C = (h_3 - h_2) + r(\cos \alpha_3 - \cos \alpha_2) - L_2 \sin \theta_2 \tag{7}$$

These equations allow to determine θ_i angles; each equation provides two configurations characterized by having points E and D symmetrically placed with respect to the segments A-B and E-C, respectively. Discarding the solutions with lower *z*-coordinate, the suspension configuration and the ground reactions can be defined.

2.2 *Examples of load distributions*

The following diagrams were obtained with reference to a small-sized rover, whose main dimensions are reported in Fig. 7 and Table I; furthermore, it was assumed that gravity acceleration is equal to 9.81 m/s², the body-payload mass of half rover 0.50 kg, the mass of each wheel-motor unit 0.052 kg, and rocker and bogie masses negligible with respect to the masses of the body-payload and of the wheel-motor assemblies. Furthermore, body-payload mass was considered as lumped in point D and the wheel-motor masses lumped in the center of each wheel. By imposing the conditions of static equilibrium, the ground reactions were calculated for different ground profiles; as examples, Fig. 8 reports three cases that can occur if the rover overcomes a step obstacle while Fig. 9(a) and 9(b) shows the rover on a sloping ground; each case is defined by a combination of values of α_i and h_i. The last case (Fig. 9(c)) refers to a wavy ground with a wavelength equal to the wheelbase, characterized by having the axles of the wheels at the same height and the same angles α_i different from zero. For each example, the angles θ_i formed by the
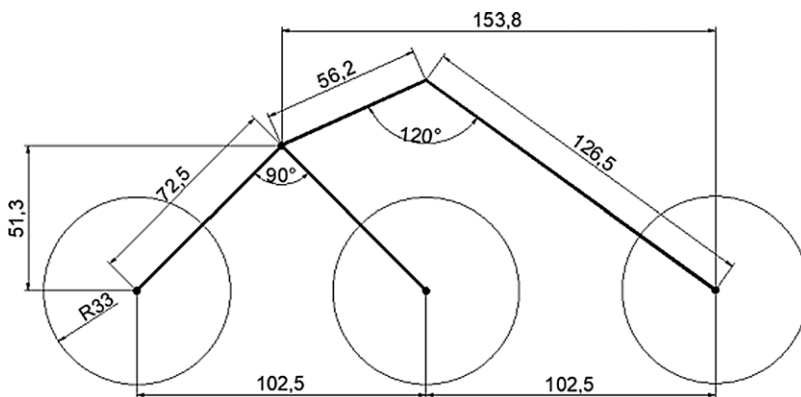
Figure 7. *Link dimensions.*

Table I. *Rover geometric characteristics.*

L1 (mm)	L2 (mm)	L3 (mm)	L4 (mm)	r (mm)	γ (deg)	β (deg)
72.5	72.5	126.46	56.23	33	90	120

Table II. *Rover configuration and soil reactions with* $\alpha_1 = \alpha_2 = \alpha_3 = 0°$.

Config.	θ_1 (deg)	θ_2 (deg)	θ_3 (deg)	θ_4 (deg)	ψ (deg)	R_a (N)	R_b (N)	R_c (N)
a)	45,0	135,0	144,1	24,1	20,9	2,22	2,22	2,22
b)	45,0	135,0	156,0	36,0	9,0	2,34	2,34	1,97
c)	63,8	153,8	151,1	31,1	32,7	2,87	1,71	2,07

Table III. *Rover configuration and soil reactions with* $\alpha_1 = \alpha_2 = \alpha_3 \neq 0°$ ($\pm 20°$).

Config.	θ_1 (deg)	θ_2 (deg)	θ_3 (deg)	θ_4 (deg)	ψ (deg)	R_a (N)	R_b (N)	R_c (N)
a)	64,97	154,97	164,04	44,04	20,93	3,09	1,76	1.81
b)	25,04	115,04	124,11	4,11	20,94	1,46	2,45	2,75
c)	45,01	135,01	144,07	24,07	20,93	2,22	2,22	2,22
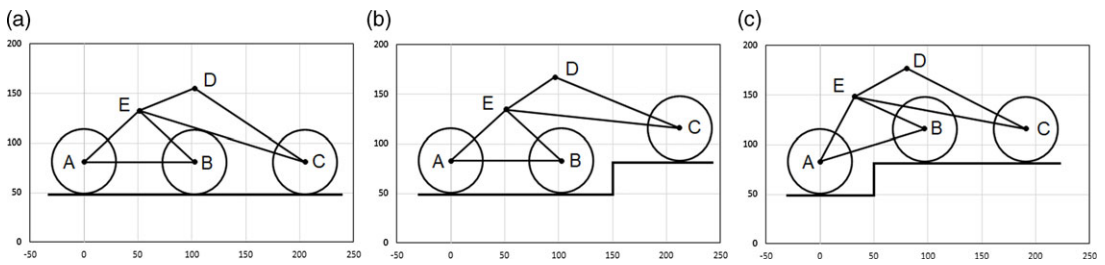
Figure 8. *Rover configurations for* $\alpha_1 = \alpha_2 = \alpha_3 = 0°$: *(a) wheels at the same level on horizontal ground; (b) wheel C placed at a higher level than the other two wheels; (c) wheels B and C at a higher level.*
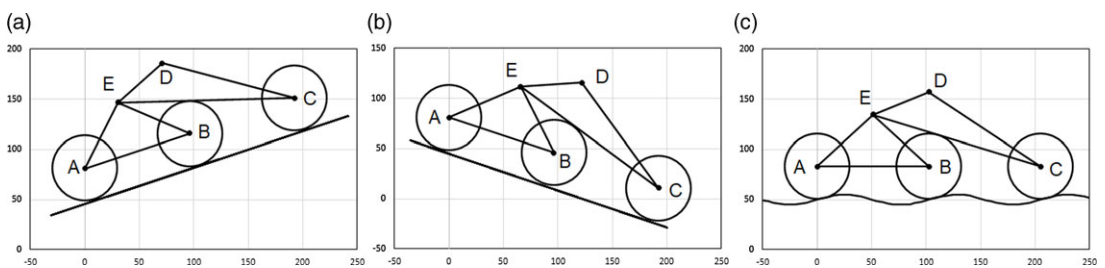
Figure 9. *Rover configurations for* $\alpha_1 = \alpha_2 = \alpha_3 \neq 0°$: *(a) (b) wheels on sloping ground and (c) wheels at the same level on locally inclined ground.*

suspension links with respect to the reference x axis and the vertical ground reactions were determined and reported in Tables II and III.

Finally, considering the whole mass lumped in point D, Fig. 10(a) shows the normal ground reactions versus the ground angle inclination, α. The interval of α was chosen so that it ranges between the values for which the vertical projection of point E passes through contact point of wheel A or B. Out of this range, the normal reactions R_{AN} or R_{BN} become zero. Although these are static considerations, referring to bogie forward direction of travel (from right to left in the figure), α positive means that the rover proceeds downhill. If the body/payload mass is lumped in D while each wheel-motor mass is lumped
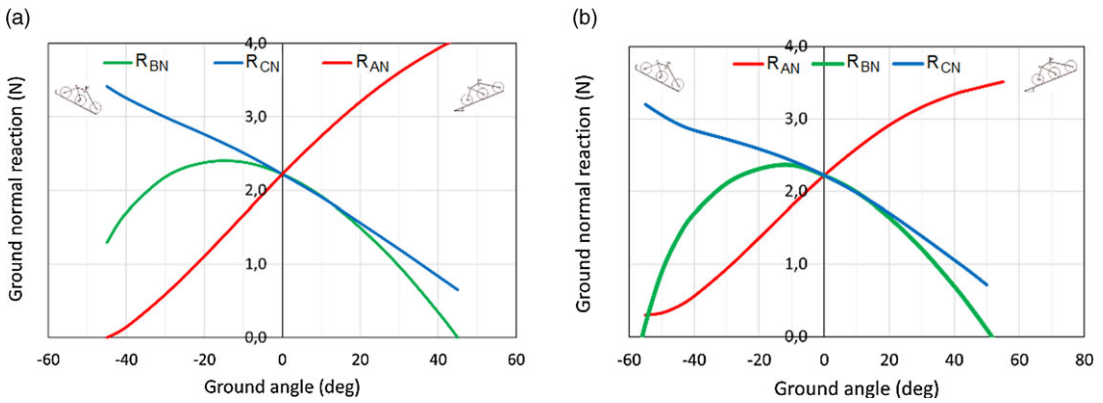
Figure 10. *Normal ground reaction: (a) with whole rover mass lumped in point D and (b) considering the wheel-motor masses lumped in A, B, C.*

in the corresponding axis of the wheels, due to the stabilizing effect of the wheel-motor weights, the rover exhibits a larger range of α for which both reactions (R_{AN}, R_{BN}) are greater than zero (Fig. 10(b)). Therefore, the assumption of considering the whole mass lumped in point D is more conservative.

3. Wheel traction force

In case of soft soil, the wheels tend to slip and to sink with the risk that the rover gets stuck. The maximum traction force is often modeled with Mohr–Coulomb formula [20] that expresses limit shear stress beyond which the wheel slips:

$$\tau_{max} = c + \sigma \tan \varphi = c + f\sigma \tag{8}$$

where c is the soil cohesivity, σ is the normal stress (pressure), ϕ is the soil's friction angle, and $f = \tan \varphi$ is the friction coefficient. The maximum driving force, depending on the shear resistance of the soil elements between consecutive cleats (or grousers), can be obtained by integrating the shear stress over the contact area A (Fig. 11(a)):

$$T_{max} = cA + fN \tag{9}$$

This expression shows that the maximum driving force increases with the contact area (Fig. 11(b)), thanks to the cohesive component; the increment of the contact area will also reduce wheel sinking.

The wheels of space rovers, adopted for Mars missions, are made of an aluminum alloy rim, with protruding cleats, connected to the hub by means of curved spokes in titanium alloy [21]. By choosing appropriate shapes and sizes of the components, the wheel will have a desired radial deformability and a desired extension of the patch contact area, as it happens for tired vehicle where the extension of the patch area is due to the radial deformability of the tire. Adequate extension of the contact area will
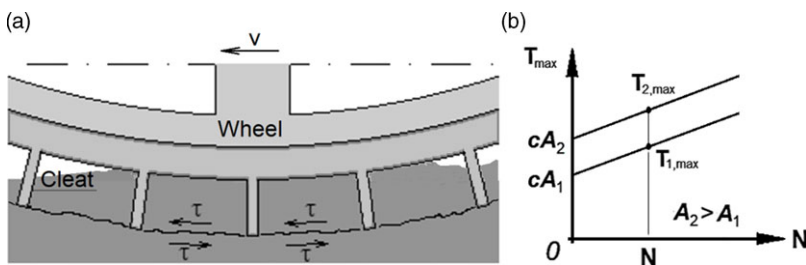
Figure 11. *Wheel-ground maximum driving force.*

increase traction capacity and will limit wheel sinking on soft soils. To avoid differences in traction and wheel sinking, the suspension system must ensure equal distribution of the load on the wheels.

The cleats protruding from the rim must guarantee a good transmission of the longitudinal force. On soft soils, they penetrate the soil and the transmission of force depends on the shear resistance of the soil between two consecutive cleats. On rocky soils, the cleats harpoon on the roughness of the soil and must resist concentrated mechanical actions and wear. The criterion for defining cleats with a rectangular section, parallel to the axis of the wheel, is reported in ref. [21]. In some cases, with the aim of improving mechanical and wear resistance, they have been made with different patterns (diagonal, sinusoidal, ecc.) [22]. In ref. [23], an interesting survey on the experimental characterization of the terrain of celestial bodies and the detection of obstacles that can be encountered by a rover along its path is reported. For the subsequent evaluations, it is assumed that the cohesion is zero and that the traction force depends only on the friction component as it occurs for incoherent soils (sandy), widespread on Martian soil.

4. Front wheel approaching an obstacle

It is assumed that the rover weight acts at point D and that it is equally distributed between the wheels in the case of flat and horizontal ground. If the front wheel of the bogie is pressed against an obstacle constituted by a vertical surface, whose height is equal or greater than the radius of the wheel (Fig. 12), the vertical reactions of the soil are no more equally distributed.

Thanks to the pushing actions provided by the rear driving wheels (F_B and F_C), it can be assumed that the contact force between wheel A and the horizontal ground is negligible, in comparison to the force exchanged with the vertical surface, and that the friction force acting in the contact point A' can support the vertical load acting on wheel A. To prevent the front wheel from slipping, the magnitude of the vertical reaction must satisfy the following condition:

$$R_{AZ} \leq f R_{AX} = f(F_B + F_C) \tag{10}$$

At the same time, to avoid the rear wheels slippage, the pushing forces magnitudes must be lower than the corresponding grip limit:

$$F_B \leq f R_{BZ}; F_C \leq f R_{CZ} \tag{11}$$

With reference to Fig. 12, indicating with h the bogie height and with L the horizontal distance between wheel C axis and hinge E when the three wheels are at the same level, from the static equilibrium condition, the rover external and internal reactions can be evaluated:

rocker equilibrium:

$$R'_{CZ} = \frac{W}{3} + F_C \frac{h+r}{L}; R'_{EZ} = \frac{2W}{3} - F_C \frac{h+r}{L}; R'_{EX} = F_C \tag{12}$$
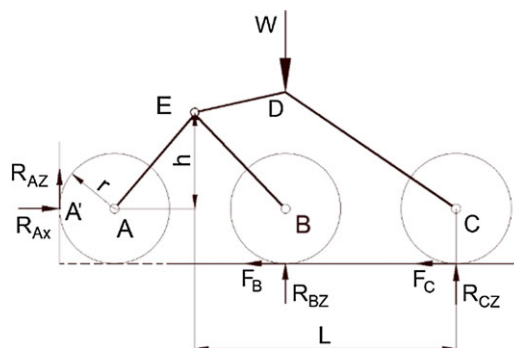
Figure 12. *Wheel A approaching the obstacle.*

(a)   (b)   (c)
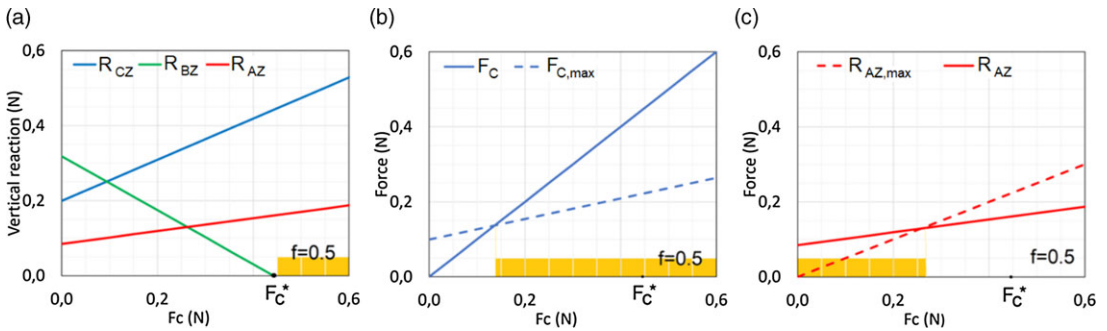
Figure 13. *Vertical soil reactions for f = 0.5 and $F_B = 0$.*
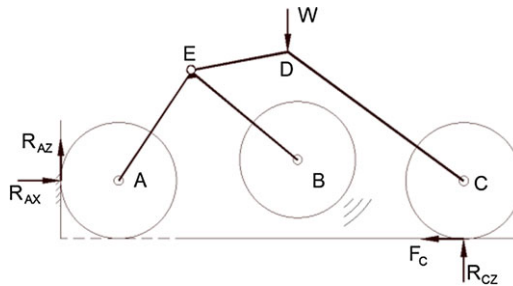
Figure 14. *Rover pose for $F_c > F_c*$.*

bogie equilibrium:

$$R'_{BZ} = \frac{R_{EZ}\left(\frac{L}{3} + r\right) + F_B r - F_C h}{\frac{2}{3}L + r}; R'_{AZ} = R'_{EZ} - R'_{BZ}; R'_{AX} = F_B + F_C \tag{13}$$

To highlight the influence of the driving actions on the ground vertical reactions, it is assumed that wheel C pushes the rover with a constant driving force while F_B is considered idler. With reference to Table I and therefore for $L = 153.75$ mm; $h = 51.27$ mm, considering $W = 0.656$ N (half rover weight) and $f = 0.5$, the ground vertical reactions were plotted (Fig. 13(a)) for increasing values of F_C. The diagram shows that as the force F_C increases, the vertical reaction of the intermediate wheel B decreases and, for $F_C > F_C^*$, it becomes null (Fig. 14). Since the wheel-soil constraint is unidirectional, the deduced reactions are no longer valid beyond F_C*. By comparing (Fig. 13(b),(c) F_C and R_{AZ} friction forces with the corresponding limit grip values ($F_{C,\max}$ and $R_{AZ,\max}$), it can be noted that R_{AZ} becomes lower than the limit grip only for $F_C > F_C*$; therefore, wheel A is unable to begin the climbing phase.

To overcome the obstacle, a higher friction coefficient is required (Fig. 15); for $f = 1$, the values of the vertical reactions needed to balance the vertical load W do not change but there is a range of F_C, lower than F_C*, for which R_{AZ} is lower than the grip limit so that wheel C does not slip. As the friction coefficient depends on the soil characteristics, in the presence of poor soil characteristics, this scenario may not occur. In the figures, a lower colored band indicates the *out-of-range F_C* values for which F_B force is negative or for which a grip limit has been exceeded; in both cases, the rover is unable to begin the overcoming of the obstacle.

The horizontal pushing force can be increased by activating the intermediate wheel B; the F_B driving force provides a moment which opposes the counterclockwise rotation of the bogie, increasing the value of the F_C*. The diagrams of the ground reactions (Fig. 16), obtained for $f = 0.5$ and $F_B = 0.05$ N, show that the value $Fc*$ is slightly increased and that F_c does not exceed the grip limit for values slightly lower than $Fc*$; in this case, R_{AZ} exceeds the grip limit. Therefore, even when wheel B is activated, a higher value of the friction coefficient is required to start the climbing phase.
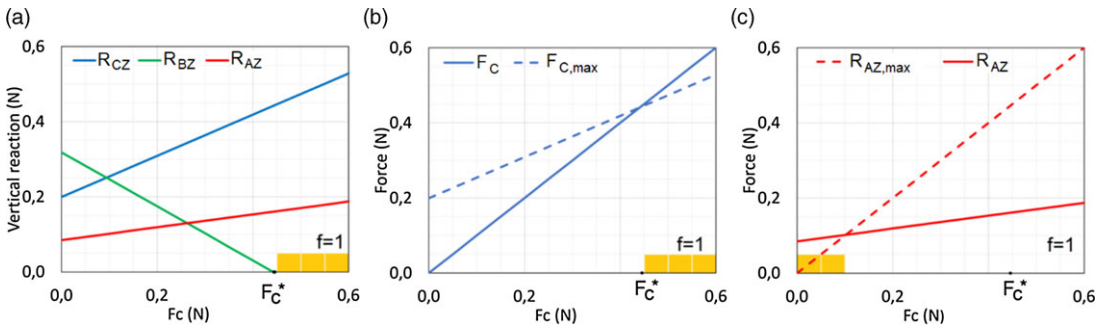
Figure 15. *Vertical soil reactions for f = 1.0 and $F_b = 0$.*
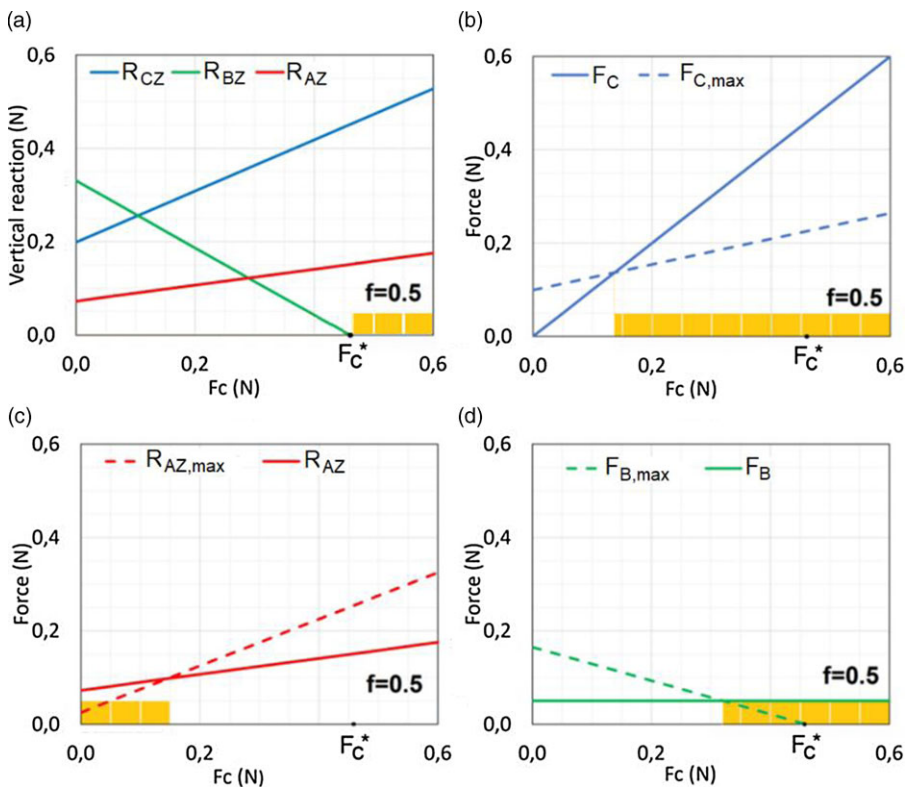
Figure 16. *Vertical ground reactions for f = 0,5 and $F_b = 0.05$ N.*

5. Rotational spring between rocker and bogie

To avoid the slippage of wheel B, it must be more loaded. To this end, it would be possible to modify the geometry of the bogie so that the load on wheel B is always greater than that of wheel A (Fig. 17(a)); the drawback of this configuration is that the front wheel would lose traction when the rover moves in the absence of obstacles; moreover, in case of unevenness ground, wheel B axis could exceed the vertical projection of point E with the risk of bogie overturning. To modify the load on the wheels of the bogie, it would be possible to equip hinge E with a torsion spring (Fig. 17(b)) giving an elastic moment:

$$M_K = M_{k0} + k\Delta\psi \tag{14}$$
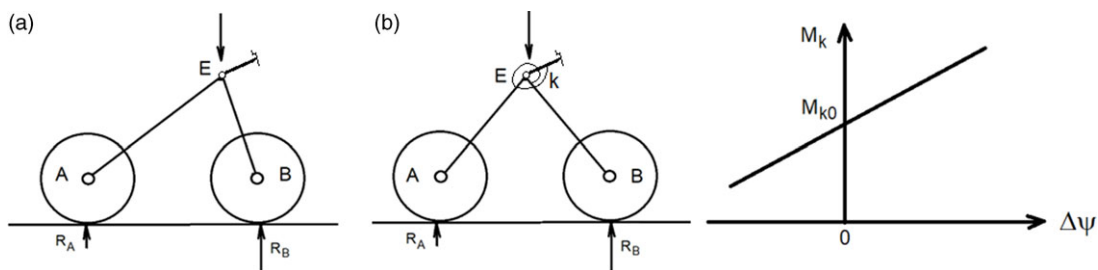
Figure 17. *(a) Asymmetrical bogie and (b) symmetrical bogie with torsion spring in hinge E.*

where M_{k0} is the spring preload, k is the torsional stiffness, and $\Delta\psi = \psi - \psi_0$ is the ψ angle variation (defined in Fig. 6) with respect to the value that it assumes when the wheels are on flat and horizontal plane. The preload must be chosen in order to limit the reduction of the load on the wheels. If the loads on the wheels assume values that are too different from each other, as mentioned, the operating conditions worsen in terms of traction and sinking capacity. As shown below, by limiting the variation of the vertical loads on the wheels, it is possible to achieve the conditions which allow to overcome an obstacle with a height greater than the wheel radius. Due to the presence of the spring, the rocker-bogie suspension can no longer be considered a pure kinematic suspension although, in this case, the spring does not have the function it assumes in dynamic suspensions, as mentioned in the introduction.

5.1 Rover on sloping ground

In the case of sloping ground, the ground reactions assume the trend shown in Fig. 18. The comparison with the diagrams reported in Fig. 10 shows that the presence of the torsion spring has the effect of slightly reducing the range of the ground angle inclination α for which both reactions (R_{AN}, R_{BN}) are greater than zero in the case of negative sloping angles and increasing it in case of positive angles.
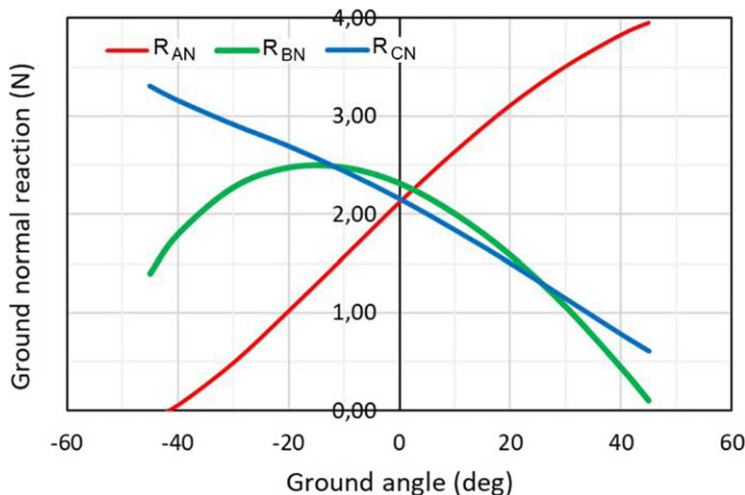
Figure 18. *Normal ground reaction with whole rover mass lumped in point D in case of torsion spring in E whose preload is equal to 10 Nmm.*

5.2 Wheel A pressed against the obstacle

The presence of a torsion spring, with adjustable preload, placed between the rocker and the bogie, in correspondence of hinge E, is here considered in the case of flat and horizontal soil with step obstacle.

In this pose, being all the wheels at the same level, $\Delta\psi$ angle is null and the elastic moment is equal to the preload M_{k0}; its value can be assigned so that the spring provides a clockwise moment on the bogie and a counterclockwise one on the rocker, with the effect of reducing the vertical load on wheels A and C and increasing it in the central wheel B. The vertical soil reactions (Fig. 12) are redistributed by considering the following additional terms in their expressions:

$$R_{CZ}^k = -\frac{M_{K0}}{L}; R_{BZ}^k = \frac{M_{K0}}{L} \cdot \frac{4L+3r}{2L+3r}; R_{AZ}^k = -\frac{2M_{K0}}{2L+3r} \tag{15}$$

From the equilibrium conditions, it follows:

$$R_{AZ}' = \frac{2W}{3} - F_C\frac{h+r}{L} - \frac{2W}{3} - F_C\frac{h+r}{L} - \frac{2M_{K0}}{2L+3r} \qquad R_{BZ}' = \frac{R_{EZ}\left(\frac{L}{3}+r\right) + F_Br - F_Ch}{\frac{2}{3}L+r} + \frac{M_{K0}}{L} \cdot \frac{4L+3r}{2L+3r}$$

$$R_{CZ}' = \frac{W}{3} + F_C\frac{h+r}{L} - \frac{M_{K0}}{L} \tag{16}$$

Diagrams of Fig. 19, obtained for $M_{K0} = 3$ Nmm, $k = 20$ Nmm/rad and $F_B = 0.1$ N, show that the tangential force of each wheel is lower than the corresponding grip limit; therefore, wheel A can begin the climbing phase.

The preloaded torsion spring increases the driving capacity of wheel B and reduces that of wheel C. This circumstance facilitates the initial climbing phase of wheel A since the force Fc generates a horizontal load in hinge E which opposes the clockwise rotation of the bogie while the driving force F_B facilitates it.
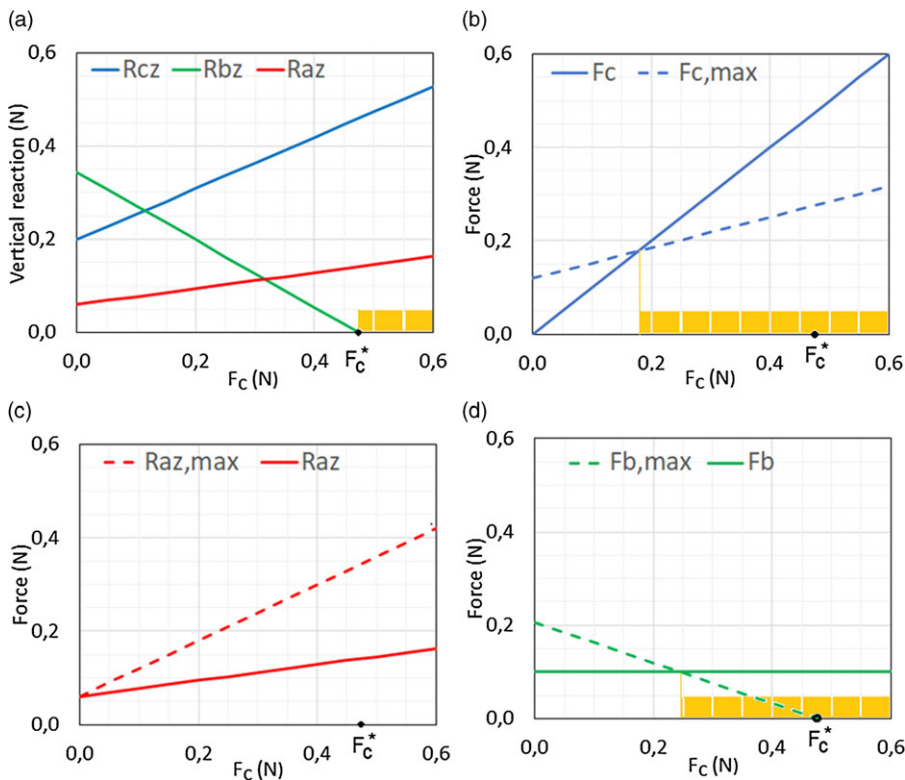
Figure 19. *Effect of the preloaded torsion spring ($F_b = 0.1$ N; $M_{k0} = 3$ Nmm; $f = 0.5$).*

5.3 Wheel B pressed against the obstacle

It is considered that the front wheel A has climbed the step obstacle whose height is equal to the radius of the wheels (Fig. 20). In this pose, the relative angle $\Delta\psi$, between rocker and bogie, is negative and the elastic moment M_k can be considered equal to zero; the angles θ_i and the soil reactions assume the values reported in Table IV.

Wheel B is pressed against the vertical surface of the step obstacle by the driving forces exerted by wheels A and C. Similarly to the previous case, it is assumed that the contact force between wheel B and the horizontal surface is negligible and that the vertical friction force is able to sustain the wheel if:

$$R_{BZ} \leq fR_{BX} = f(F_A + F_C); F_A + F_C \leq f(R_{AZ} + R_{CZ}) \tag{17}$$

Considering wheel A idler, the traction force F_C, required to overcome the obstacle, is evaluated; the traction capacity of the wheels depends on the normal ground reactions having the following expressions:

$$R_{CZ} = W\frac{(DE)_x}{(EC)_x}; R_{EZ} = W\frac{(DC)_x}{(EC)_x}; R_{AZ} = R_{EZ}\frac{(EB)_x}{(AB)_x}; R_{BZ} = R_{EZ}\frac{(AE)_x}{(AB)_x} \tag{18}$$

The subscript "*x*" indicates the projection of each segment on the horizontal *x*-axis, where:

$$(DC)_x = DC\cos(\pi - \theta_3); (DE)_x = DE\cos\theta_4; (EC)_x = (DC)_x + (DE)_x \tag{19}$$

The trends of the soil vertical reactions, versus the F_C force, are reported in Fig. 21. It shows that the F_C force must be high enough to have R_{BZ} values lower than the grip limit (Fig. 21(d)); in any case, F_C is lower than the grip limit. Reaction R_{AZ} grows with F_C (so that wheel A could take on a higher drive capacity; in this case it is considered idler). Due to the relative rotation between rocker and bogie, the elastic moment from the torsion spring preload is reduced.

By activating wheel A (Fig. 22), it can be seen that the driving capacity of wheel C does not vary while wheel A is able to provide a small contribution only for higher values of F_C. R_{BZ} reaction also increases as the force that keeps the wheel pushed against the obstacle is higher.

The diagrams show that with only the driving action of wheel C the rover has the possibility to start the climbing phase of wheel B.

Table IV. *Rover pose and soil vertical reactions with wheel A over the obstacle.*

θ_1 (deg)	θ_2 (deg)	θ_3 (deg)	θ_4 (deg)	ψ (deg)	R_a (N)	R_b (N)	R_c (N)
26,2	116	139	18,9	7,37	1,62	2,69	2,34
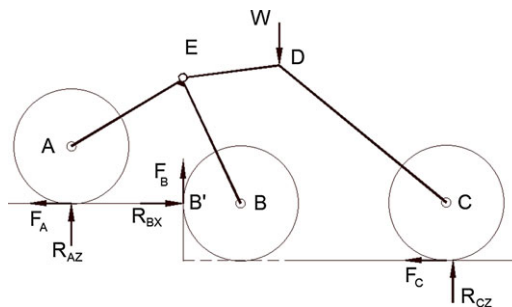
Figure 20. *Wheel B approaching the obstacle ($h_1=r$; $h_2=h_3=0$).*
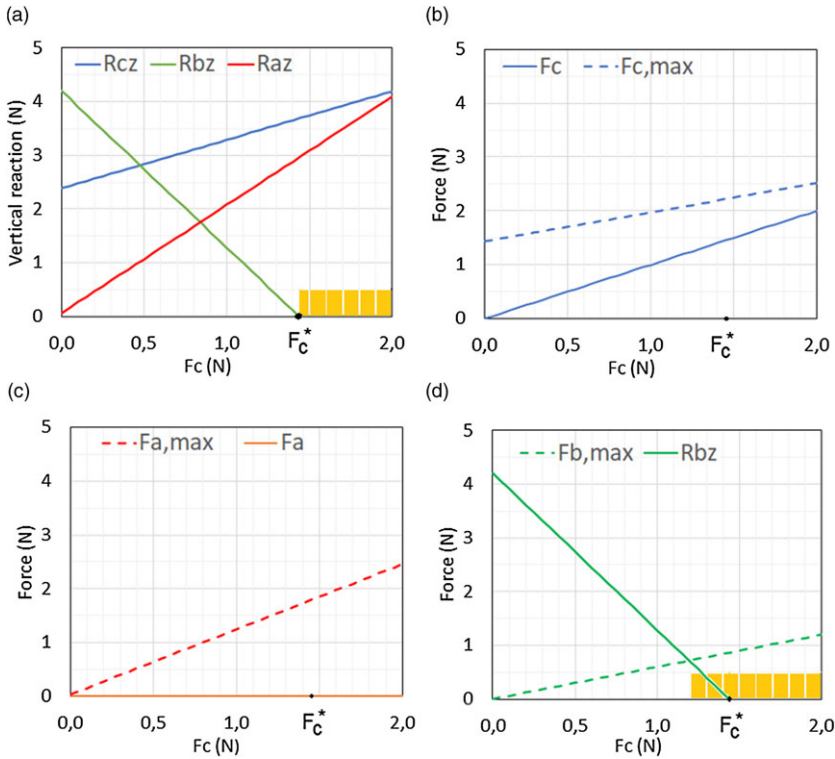
Figure 21. *Wheel B approaching the obstacle without torsion spring and wheel A idler.*
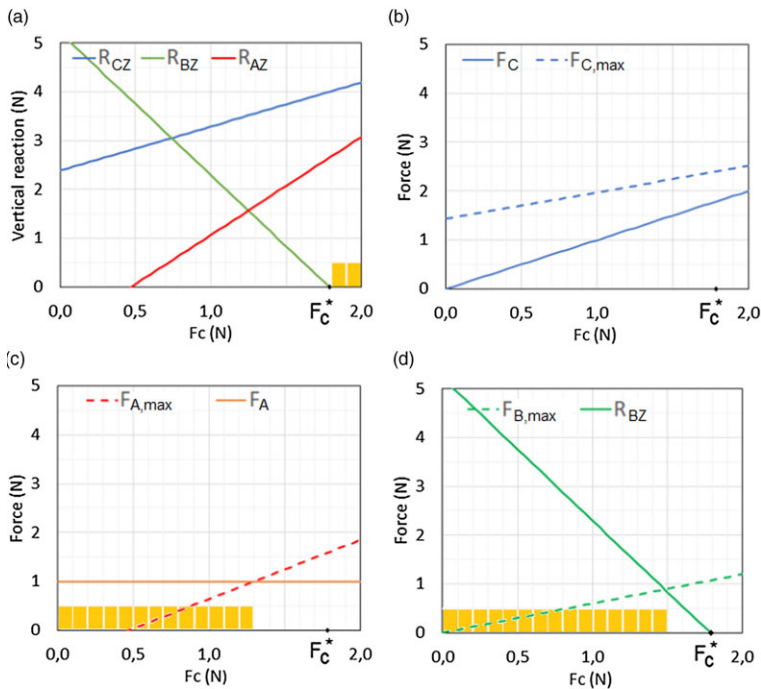
Figure 22. *Wheel B approaching the obstacle without torsion spring and $F_A = 1$ N.*
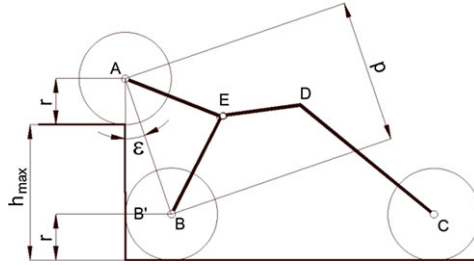
Figure 23. *Theoretical maximum height that can be overcome.*

Regardless of the presence of the spring, the geometric theoretical maximum height of the obstacle step that a rover can overcome [24] is defined as the one for which wheel A is on the obstacle, with wheel B at the beginning of the climbing phase (Fig. 23):

$h_{\max} = p \cos \varepsilon$, with:

$$\varepsilon = \arcsin \left(\frac{r}{p} \right) \tag{20}$$

where p is the distance between wheels A and B axes.

5.4 Wheel C pressed against the obstacle

Finally, the last phase which concerns the climbing phase of wheel C is considered (Fig. 24). In this case, the driving action of one of the two bogie wheels must be considered; the driving action of wheel B is chosen as it is the more loaded wheel of the bogie. For this condition, the angles θ_i defining the rover pose and the ground reactions are reported in Table V. Considering wheel C pushed against the step obstacle, the external and internal constraint reactions are

$$R_{CX} = R_{EX} = F_A + F_B; R_{CZ} = \frac{W(DE)_x - (F_A + F_B)(EC)_z - M_k}{(EC)_x - r}; R_{EZ} = W - R_{CZ};$$

$$R_{BZ} = \frac{F_B[r + (EB)_z +]R_{EZ}(AE)_x - F_A\left[r + (EA)_z\right] - M_k}{(AB)_x}; R_{AZ} = R_{EZ} - R_{BZ} \tag{21}$$
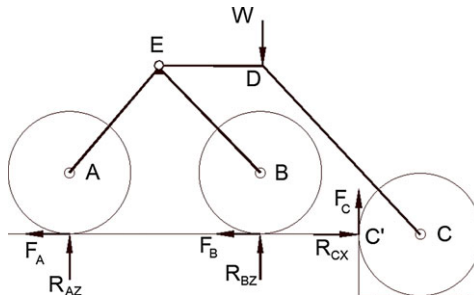
Figure 24. *Wheel C approaching the obstacle.*

Table V. *Rover pose and soil vertical reactions with wheel A and B over the obstacle.*

θ_1 (deg)	θ_2 (deg)	θ_3 (deg)	θ_4 (deg)	ψ (deg)	R_A (N)	R_B (N)	R_C (N)
45,0	135	131	11,2	33,8	2,06	2,06	2,54
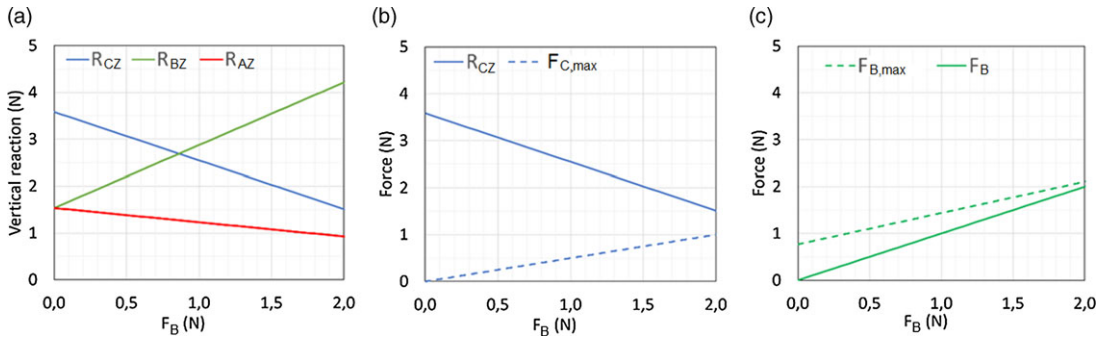
Figure 25. *Wheel C approaching the obstacle without the effect of the torsion spring.*
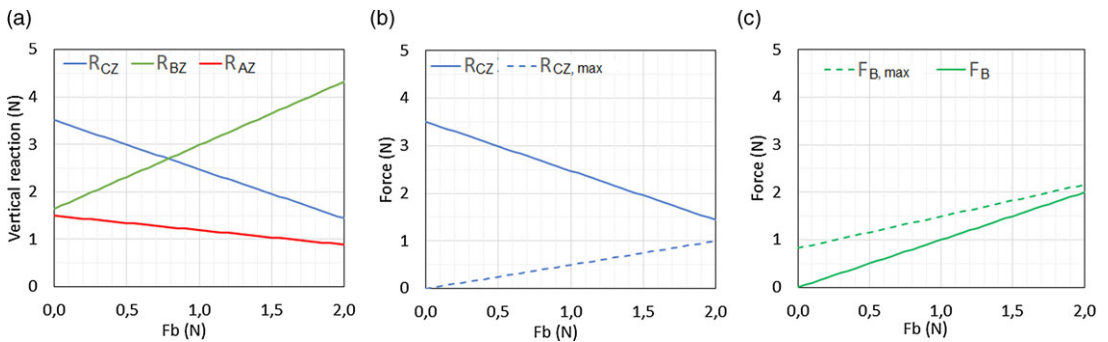
Figure 26. *Wheel C approaching the obstacle with $M_{k0} = 3$ Nmm; $k = 20$ Nmm/rad.*

with:

$$R_{CZ} \leq fR_{CX} = f(F_A + F_B); \; F_A + F_B \leq f(R_{AZ} + R_{BZ})$$

The vertical soil reactions are plotted in Fig. 25 without considering the spring effect; the diagrams show that the vertical reaction of the intermediate wheel increases with F_B remaining in grip condition while the vertical friction of wheel C decreases with F_B.

The horizontal reactions R_{CX} and R_{EX} tend to rotate the rocker counterclockwise allowing the rover to undertake the last phase of overcoming the obstacle.

In this pose, angle $\Delta \psi$ is positive and the elastic moment M_k is therefore greater than M_{k0}; the moment has the effect of increasing the vertical load on wheel B, which is thus able to provide a higher driving force (Fig. 26); at the same time, due to the elastic moment, wheel C is less pressed on the vertical surface of the obstacle. The presence of the preloaded torsion spring leads to a slight increase in R_{BZ} and a slight decrease in R_{AZ} and R_{CZ}.

6. The multibody model

To verify the behavior of the proposed modified rocker-bogie suspension, a multibody model of a small prototype of a six wheels rover was developed in Simscape Multibody™ (Mathworks) environment (Fig. 27). In addition to the dynamics of the model, several physical domains were analyzed simultaneously: the electromagnetics of the motors, the dynamics of the structure, and the interaction with the ground.

The model considers the equations that describe the six independent DC motors, to perform a more realistic simulation. The six DC motors have been modeled not only with the presence of kinematic constraints but also with the presence of the equations describing their dynamics. The torques that actuate the wheels are not simple feedforward torques, but they are controlled torques, calculated on the basis of the dynamics of the electric motors.

Contact modeling is used to simulate wheel–ground interaction. At the point of contact between these two parts, it is possible to define a plane that is simultaneously tangent to the two bodies. On this plane, from the contact, we can define two distinct forces:

- the normal force, which acts in the normal direction.
- the frictional force, which acts in the tangential direction.

These forces are determined through the penalty method: a small interpenetration is achieved between the two parts to calculate the contact forces using the equation of the classic spring-damper system. The normal contact force is therefore proportional to the corresponding depth of penetration and to the velocity, both calculated along the direction of the normal.
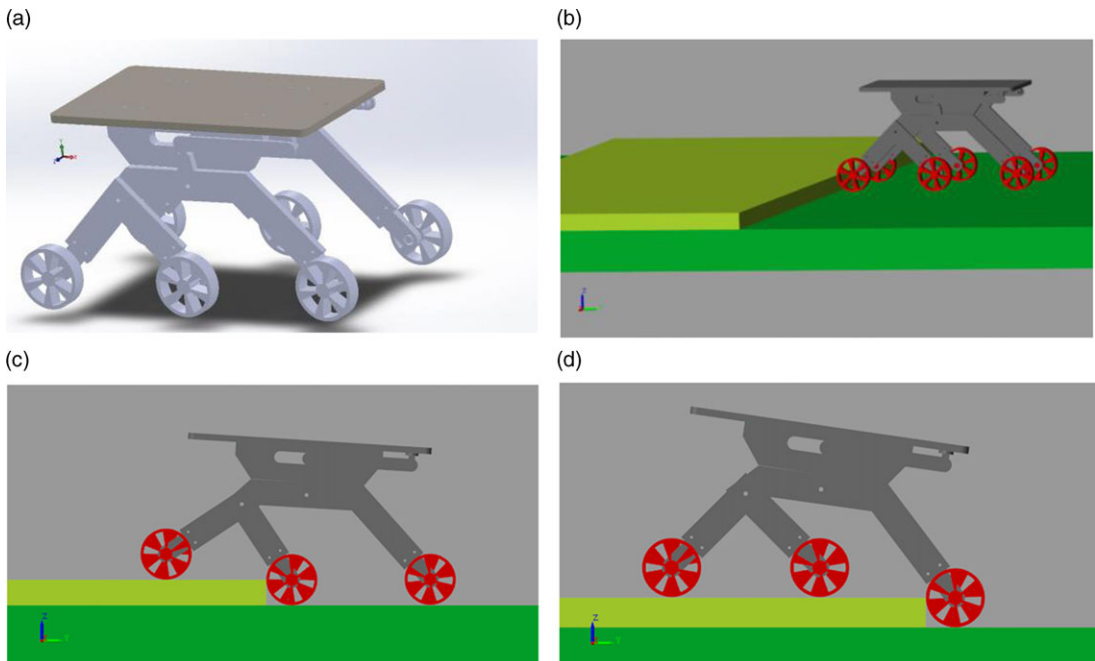
Figure 27. *(a) Robotic rover multibody model and (b)(c)(d) multibody model in three successive stages of overcoming the step obstacle.*
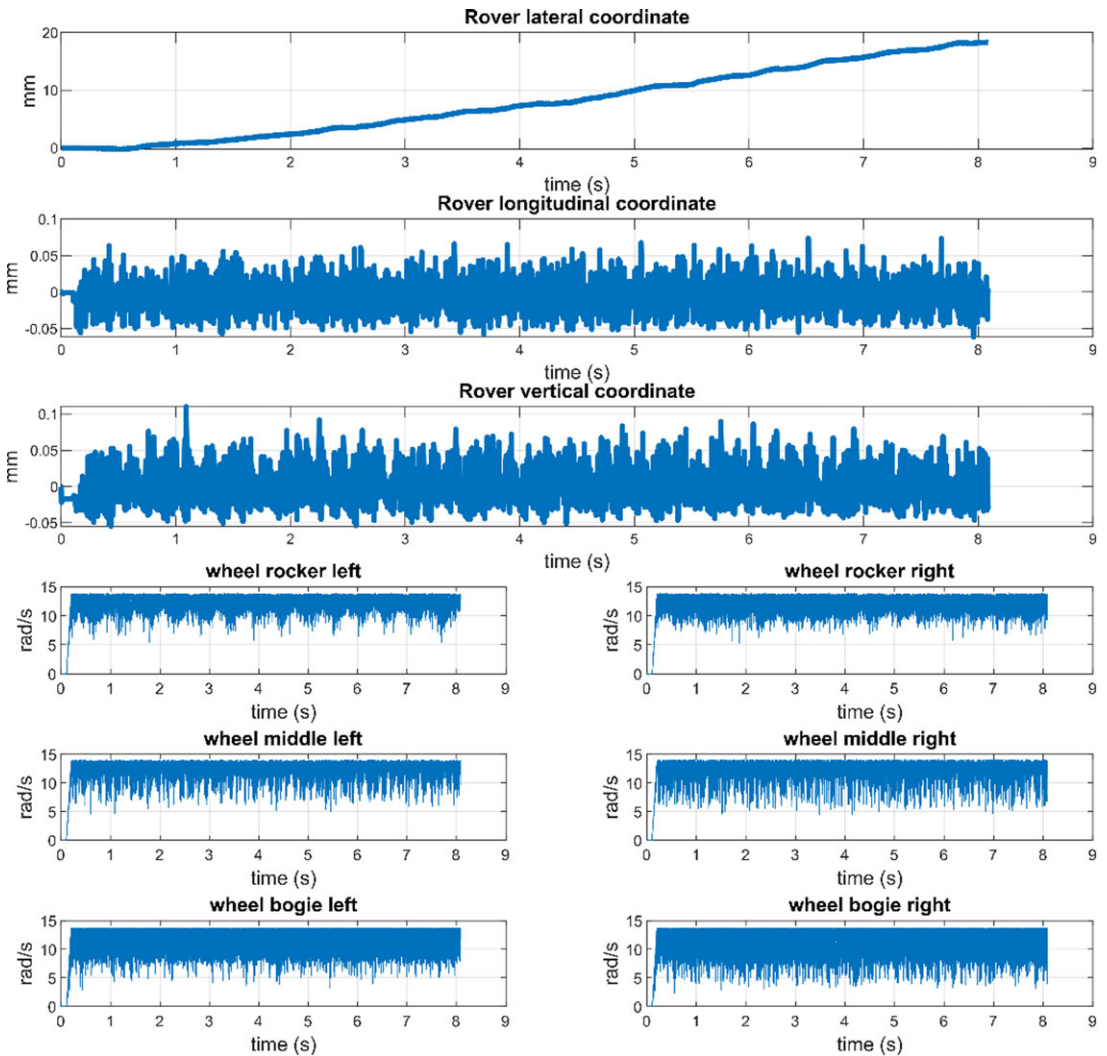
Figure 28. *Classic rocker-bogie suspension with front wheels in contact with the obstacle ($f_s = 0, 55$ and $f_d = 0, 5$).*

The frictional force was obtained through the following formulation:

$$F_a = \mu(V_r) \cdot F_n \tag{22}$$

where F_a is the friction force, F_n is the normal force, and $\mu \cdot (V_r)$ is the friction coefficient, defined in continuity as the tangential relative speed V_r varies.

The multibody model was adopted to evaluate whether the addition of the torsion spring to the rover suspension, placed between rocker and bogie, facilitates the initial phase of overcoming a step obstacle whose height is equal to the radius of the wheels. All tests were performed by running the six motors with a law of motion which increases the speed of each wheel up to its maximum value without exceeding the maximum acceleration and the torque capacity.

Without considering the torsion spring, if the front wheel (A) is in contact with the obstacle (Fig. 27(b)) and the coefficient of friction is equal to 0.55 in static condition (f_s) and 0.5 in dynamic condition (f_d) both for the soil and the obstacle, the wheels start to slip and the rover is unable to overcome the obstacle. Figure 28 shows that, even if the wheels rotate at their maximum velocity, the longitudinal
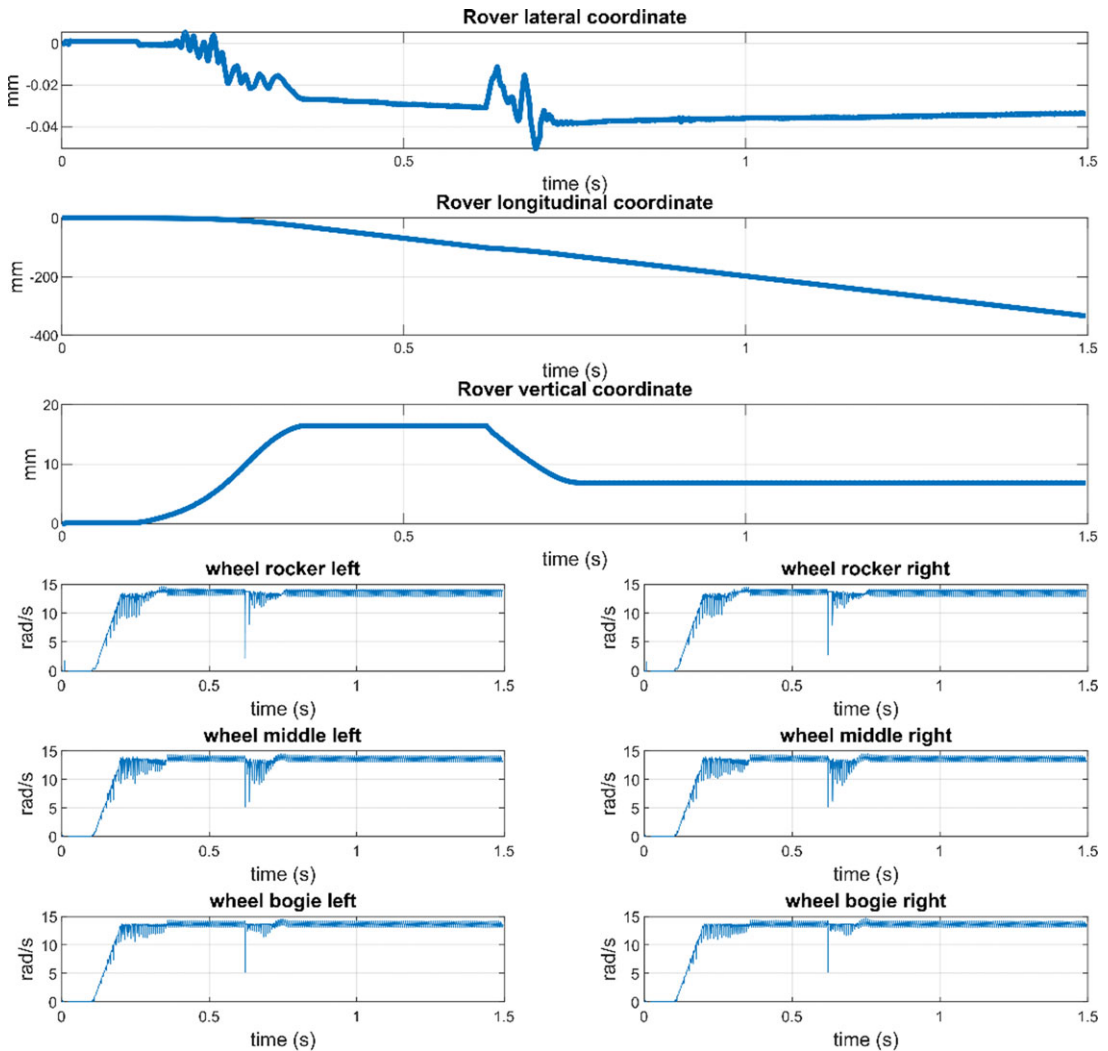
Figure 29. *Classic rocker-bogie suspension with intermediate wheels against the obstacle ($f_s = 0,55$ and $f_d = 0,5$).*

coordinate of the rover does not change. The lateral coordinate slightly changes as the wheels sliding causes a small lateral slip of the rover.

The middle wheels can overcome the obstacle if they are pressed against the obstacle and the front ones are already on it (Fig. 27(c)). Figure 29 shows that, in this case, the longitudinal position of the rover varies while the wheels rotate at their maximum speed. The rotational speed discontinuities are due to the impact of the rear wheels with the obstacle.

Even if starting with the rear wheels against the obstacle (Fig. 27(d)), the rover can move forward (Fig. 30).

These simulations demonstrate that the critical phase of overcoming an obstacle is the initial phase during which the front wheels must start to lift and climb on it. To facilitate this phase, it is necessary to reduce the vertical load on the front wheels and ensure that the other wheels have a higher driving capacity.
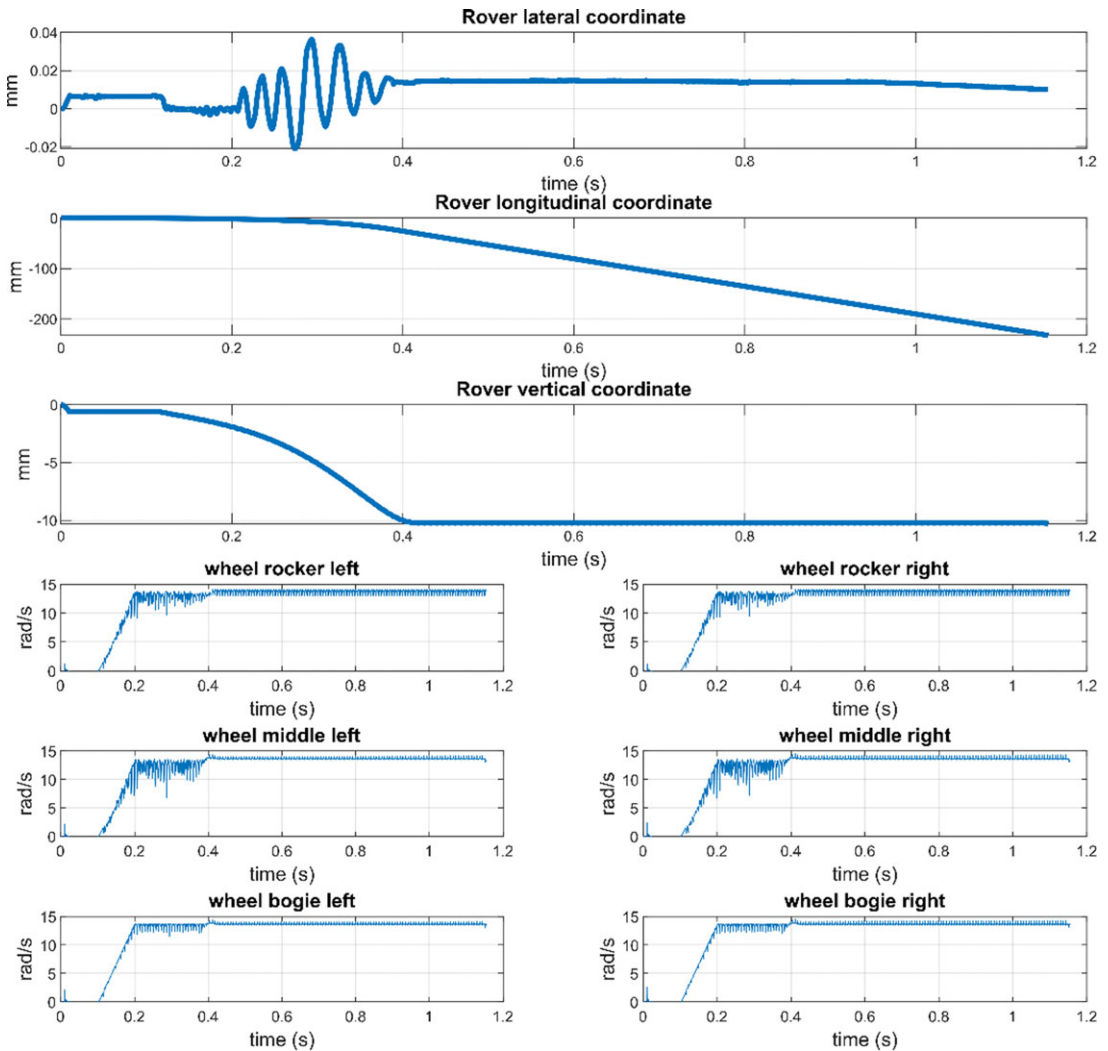
Figure 30. *Classic rocker-bogie suspension with the rear wheels against the obstacle ($f_s = 0, 55$ and $f_d = 0, 5$).*

The only way to trigger the overcoming of the obstacle, with a classic rocker-bogie suspension, is to guarantee high grip values between the wheels and the ground and the wheels and the obstacle, as shown by the results of the simulation carried out with a higher friction coefficient. As an example, Fig. 31 reports the results of a simulation in which the coefficient of friction was set equal to 0.75 in static condition and 0.7 in dynamic condition both for the soil and the obstacle; it shows that the longitudinal position of the rover changes over time as the speed of the wheels increases from zero to the maximum value; it is also possible to identify the instant in which the front wheels begin to overcome the obstacle.

Similar results are obtained for moving the rover with the rocker forward (wheel C is the first to climb the obstacle).

Since the grip conditions can only be improved within certain limits, to facilitate the phase of overcoming the obstacle, a preloaded torsion spring has been introduced between rocker and bogie to reduce the vertical load on the front wheels and increase the driving capacity of the other wheels.
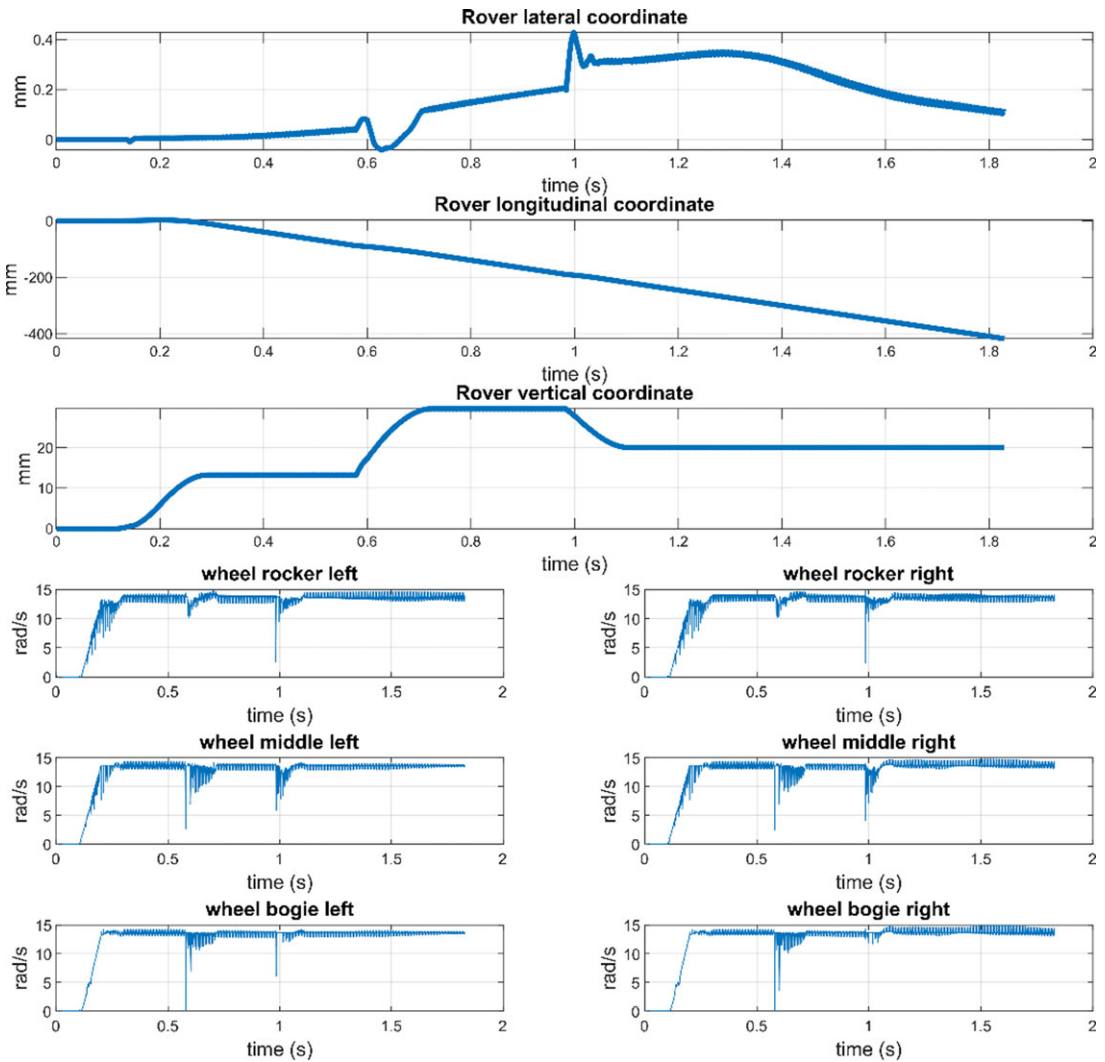
Figure 31. *Classic rocker-bogie suspension with front wheels against the obstacle ($f_s = 0,75$ and $f_d = 0,7$).*

In this condition, the simulations gave a satisfactory result even with a coefficient of friction of 0.55 in static condition and 0.5 in dynamic condition. Figure 32 shows the results obtained with a spring preload of 13.5 Nmm.

The spring preload is identified as the minimum value of M_k that is able to balance the vertical reaction on the first wheel that approaches the obstacle at the instant in which it begins to be pressed against the obstacle by the other wheels. To obtain this value of M_k, Eq. (10) can be used as an equality assuming that the driving torques on the wheels, at the instant of engagement with the obstacle, increase together in observance of the adhesion limits.

For the proposed rover model, the above minimum value of M_k is 0.0135 Nm, and in diagram of Fig. 33 it is possible to observe the reactions of Eq. (16) evaluated with this value of M_k as function of torque on wheels.
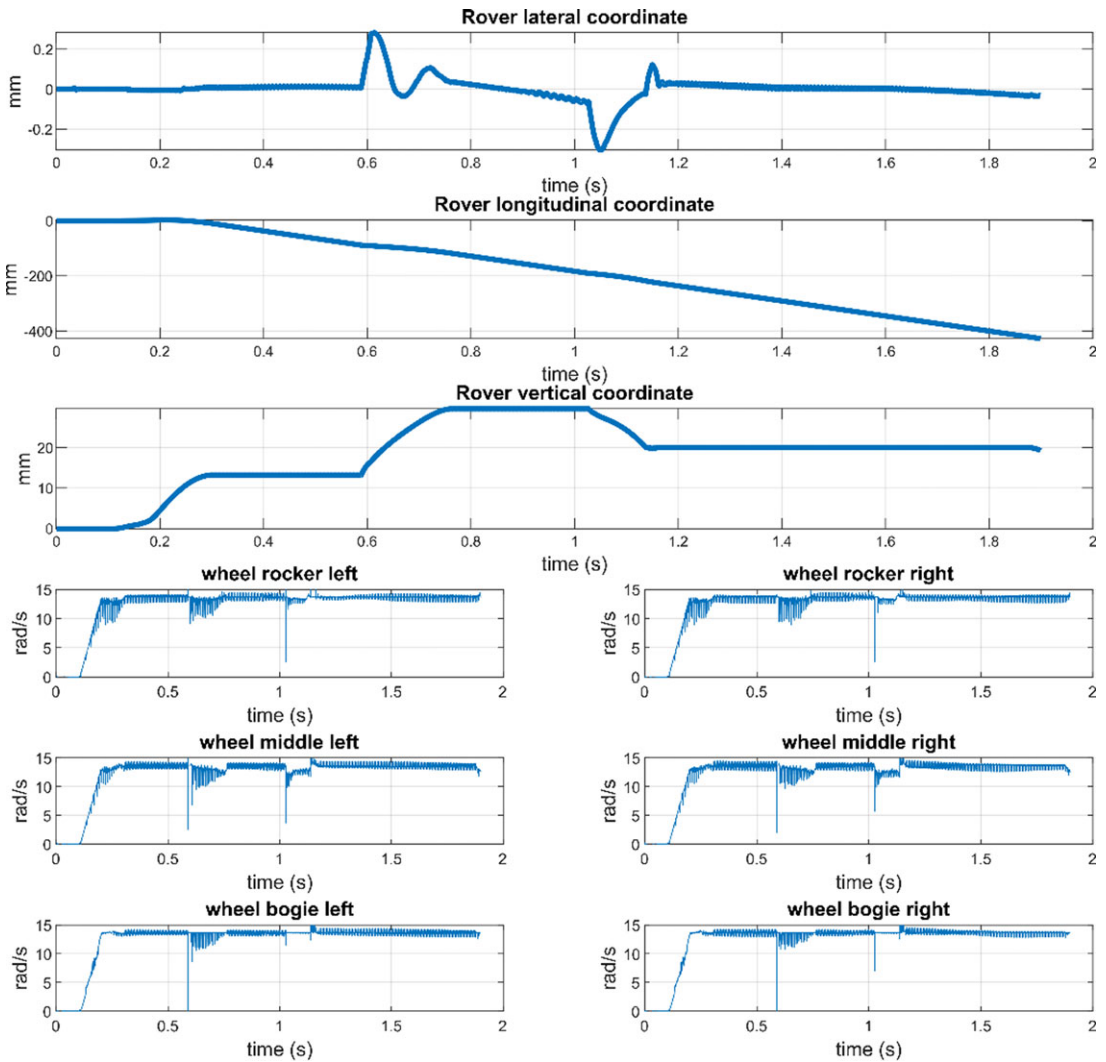
Figure 32. *Modified rocker-bogie suspension with front wheels against the obstacle ($f_s = 0,55$ and $f_d = 0,5$; $M_{k0} = 13$ Nmm).*

The spring preload produces a reduction of the load on the external wheels, while producing an increase on the middle wheels. Figure 34 reports the normal contact force between the ground and the wheels of the rover left side both in case of absence (blue line) and presence (red line) of the spring action. It is evident to observe that before the front wheel is pushed against the obstacle by the other wheels (up to 0.1 s), the action of the spring generates a different distribution of the static load on the wheels as previously mentioned.

The results of the simulation carried out with multibody model suggest that the introduction of a soft preloaded torsion spring, acting in the hinge between rocker and bogie, helps the outer wheels of the rover to overcome an obstacle. This configuration is a fundamental step to trigger the overcoming of the obstacle for the rover.
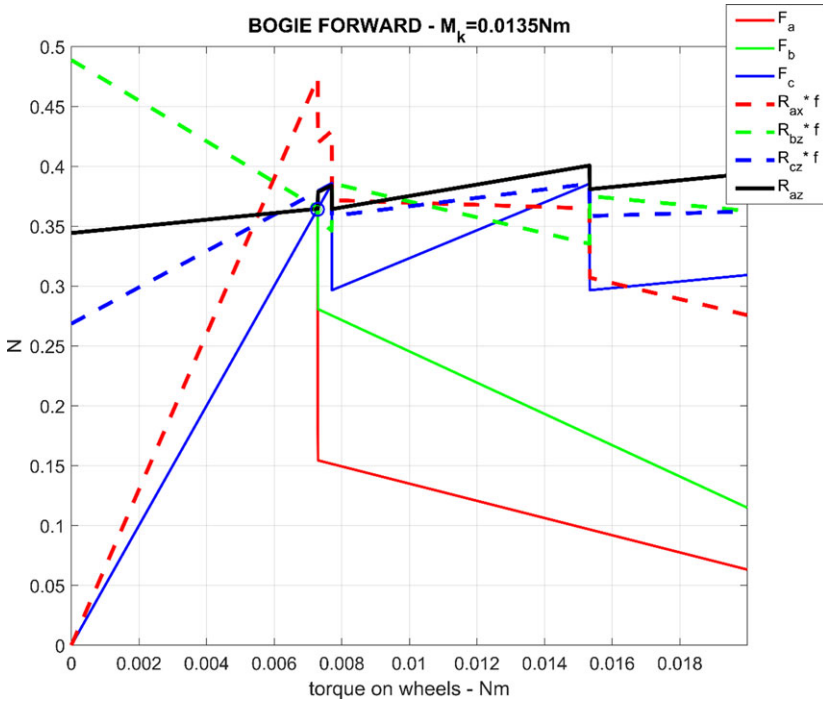
Figure 33. *-Reaction on wheels as function of torque on wheels ($f_s = 0,55$ and $f_d = 0,5$).*
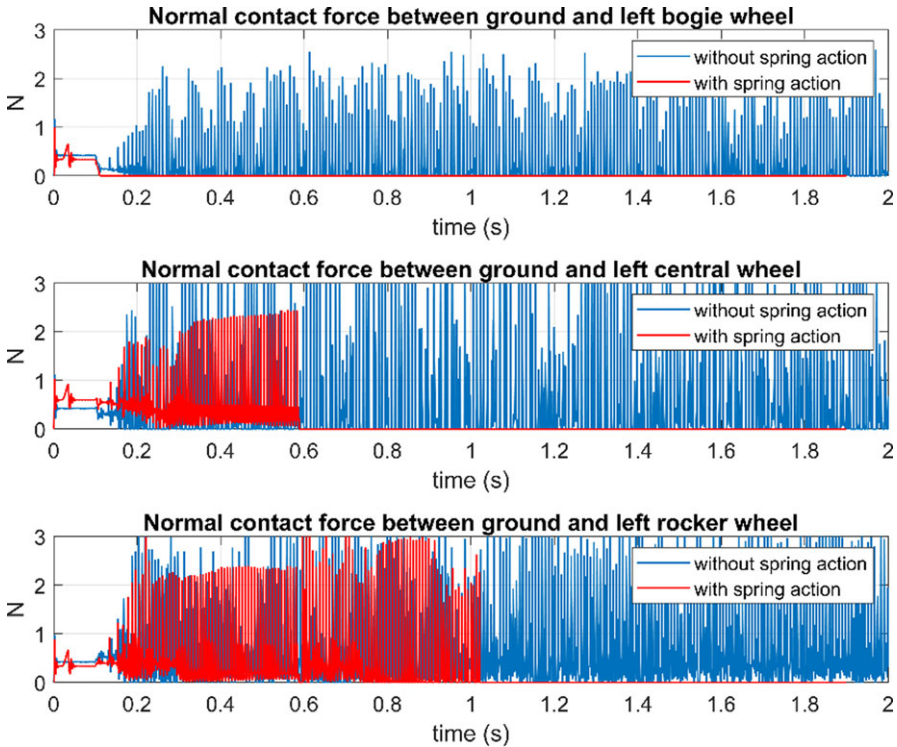
Figure 34. *-Spring preload action on wheels load repartition on left side of the rover ($f_s = 0,55$ and $f_d = 0,5$).*

7. Conclusion

The possibility of adopting a preloaded torsion spring between the rocker and bogie of the articulated suspension was considered. The spring redistributes the loads among the wheels by increasing the load on the central wheels.

Simple static evaluations show that, in the bogie forward condition, the effect of the spring is important at the beginning of the climbing phase of the front wheels allowing them to overcome the obstacle.

Once the first wheel has climbed the obstacle, the presence of the spring has small influence; in fact, when the central wheels approach the obstacle, due to the rotation of the rover, the preload becomes almost nil and, due to the low torsional stiffness, the effect of the spring is practically negligible.

Finally, when the rear wheels approach the obstacle, the presence of the spring causes a higher elastic moment, further increasing the normal load of the central wheels that are able to drag the rear wheels over the obstacle.

The paper considered the starting conditions of each phase from a standstill condition; if the dynamic effect is considered, once the front wheels have overcome the obstacle, the other two climb over it more easily. For this reason, the presence of the spring can be advantageous in the presence of uneven ground.

Through a multibody code, it has been verified that the preloaded spring between rocker and bogie provides an advantage to overcome an obstacle, as analytically foreseen.

The next steps of this study will concern an experimental investigation for the validation of the theoretical results, followed by another aspect concerning the possibility of using this solution also to facilitate skid steering. In fact, the preloaded spring has the effect of reducing the load on the front and rear wheels and therefore to reduce the modulus of the transversal actions which oppose the change in direction of the rover. Furthermore, a motor could be used to modify the spring preload to greatly facilitate skid steering or to facilitate the overcoming of an obstacle. In this way, it would be possible to avoid the use of the four motors which, in some types of rovers (e.g. space rovers), are used to steer the four steering wheels with a considerable reduction in weight and mechanical complexity.

References

[1] P. Putz, "Space robotics in Europe: A survey," *Robot. Auton. Syst.* **23**(1-2), 3–16 (1998).
[2] https://patentimages.storage.googleapis.com/5b/28/cc/ddbc12499d99b7/US4128137.pdf.
[3] D. De Falco, G. Di Massa and S. Pagano, "On the castor dynamic behavior," *J. Frankl. Inst.* **347**(1), 116–129 (2010).
[4] D. B. Bickler, USA patent n. 4,840,394: *Available at:* https://ntrs.nasa.gov/citations/19900007837.
[5] D. B. Bickler, "Roving over mars," *Mech. Eng.* **120**(04), 74–77 (1998).
[6] B. D. Harrington and C. Voorhees, "The Challenges of Designing the Rocker-Bogie Suspension for the Mars Exploration Rover," Proceedings of 37th Aerospace Mechanisms Symposium, Johnson Space Center, May 19-21 (2004).
[7] R. A. Lindemann and C. J. Voorhees, "Mars Exploration Rover Mobility Assembly Design, Test and Performance," 2005 IEEE International Conference on Systems, Man and Cybernetics, vol. **1** (2005) pp. 450–455. doi:10.1109/ICSMC.2005.1571187.
[8] https://spaceplace.nasa.gov/mars-sojourner/en/.

[9] H. J. Eisen, C. W. Buck, G. R. Gillis-Smith and J. W. Umland, "Mechanical Design of the Mars Pathfinder Mission," 7th European Space Mechanisms and Tribology Symposium (1997).

[10] A. Ellery, N. Patel, L. Richter, R. Bertrand and J. Dalcomo, Exomars rover chassis analysis & design. Proc. of 'The 8th International Symposium on Artificial Intelligence, Robotics and Automation in Space - iSAIRAS', Munich, Germany, 5-8 September 2005 (ESA SP-603, August 2005) (2005).

[11] T. Flessa, E. W. McGookin and D. G. T. Thomson, "Systems Review and Performance Metrics of Planetary Exploration Rovers," 3th International Conference on Control, Automation, Robotics and Vision (ICARCV'14), 10-12 Dec 2014, Marina Bay Sands, Singapore (2014) pp. 1554–1559.

[12] C. Dongkyu, O. Jongkyun and K. Jongwon, "Analysis method of climbing stairs with rocker-bogie mechanism," *J. Mech. Sci. Technol.* **27**, 9 (2013).

[13] A. Nicolella, V. Niola, S. Pagano, S. Savino and M. Spirto, "An Overview on the Kinematic Analysis of the Rocker-Bogie Suspension for Six Wheeled Rovers Approaching an Obstacle," *4th IFToMM Italy Conference, Sept. 7-9, 2022, Napoli, Italy. Book: Advances in Italian Mechanism Science* (Springer Nature Switzerland AG, 2022)

[14] A Brief History of the Lunar Roving Vehicle. *Available at:* https://www.hq.nasa.gov/alsj//MSFC-LRV.pdf.

[15] T. Thueer, R. Siegwart and P. G. Backes, Planetary Vehicle Suspension Options, IEEEAC paper n.1676 (2008).

[16] P. S. Schenker, L. F. Sword, A. J. Ganino, D. B. Bickler, G. S. Hickey, D. K. Brown, E. T. Baumgartner, L. H. Matthies, B. H. Wilcox, T. Balch, H. Aghazarian and M. S. Garrett, "Lightweight Rovers for Mars Science Exploration and Sample Return," Proceedings of Intelligent Robots and Computer Vision XVI, vol. **3208** (1997).

[17] P. Palash, S. R. Vishwajeet, A. Shreesh, M. Prafful and G. Prashant, "Design of rocker-bogie mechanism for application in agriculture," *Int. J. Res. Eng. Appl. Manag. (IJREAM)* (2019), Special Issue.

[18] C. Cosenza, V. Niola, S. Pagano and S. Savino, "Spring-Loaded Rocker-Bogie Suspension for Six Wheeled Rovers," *4th IFToMM Italy Conference. Sept. 7-9, 2022, Napoli, Italy - Book: Advances in Italian Mechanism Science* (Springer Nature Switzerland AG, 2022) chapter 12

[19] F. Califano, C. Cosenza, V. Niola and S. Savino, "Multibody model for the design of a rover for agricultural applications: A preliminary study," *Machines* **10**(4), 235 (2022). Article number 235, ISSN 20751702. https://doi.org/10.3390/machines10040235.

[20] G. Genta. *Introduction to the Mechanics of Space Robots* (Springer, 2012).

[21] H. Nayar, J. Kim, B. Chamberlain-Simon, K. Carpenter, M. Hans, A. Boettcher and B. Bittner, "Design optimization of a lightweight rocker-bogie rover for ocean worlds applications," *Int. J. Adv. Robot. Syst.* **16**(6), 172988141988569 (2019).

[22] E. Ackerman and I. Necessary, "Mars rover curiosity could rip its own wheels off to stay mobile," *IEEE Spect.* (2021).

[23] H. J. Moore, D. B. Bickler, J. A. Crisp, H. J. Eisen, J. A. Gensler, A. F. C. Haldemann, J. R. Matijevic and L. K. Reid, "Soil-like deposits observed by sojourner, the pathfinder rover," *J. Geophys. Res.* **104**(e4), 8729–8746 (1999).

[24] S. Chhaniyara, C. Brunskill, B. Yeomans, M. C. Matthews, C. Saaj, S. Ransom and L. Richter, "Terrain trafficability analysis and soil mechanical property identification for planetary rovers: A survey," *J. Terramech.* **49**(2), 115–128 (2012).